# Zinc inhibition of rat NR1/NR2A *N*-methyl-D-aspartate receptors

Kevin Erreger and Stephen F. Traynelis

*Department of Pharmacology, Emory University School of Medicine, Rollins Research Center, Atlanta, GA 30322, USA*

**Zinc ions ($Zn^{2+}$) are localized in presynaptic vesicles at glutamatergic synapses and released in an activity-dependent manner. Modulation of NMDA-type glutamate receptors by extracellular $Zn^{2+}$ may play an important role under physiological conditions and during pathologies such as ischaemia or seizure. $Zn^{2+}$ inhibits NMDA receptors containing the NR2A subunit with an $IC_{50}$ value in the low nanomolar concentration range. Here we investigate at the single-channel level the mechanism of high affinity $Zn^{2+}$ inhibition of recombinant NR1/NR2A receptors expressed in HEK293 cells. $Zn^{2+}$ reversibly decreases the mean single-channel open duration and channel open probability determined in excised outside-out patches, but has no effect on single-channel current amplitude. A parallel series of experiments demonstrates that lowering extracellular pH (increasing proton concentration) has a similar effect on NR1/NR2A single-channel properties as $Zn^{2+}$. Fitting the sequence of single-channel events with kinetic models suggests that the association of $Zn^{2+}$ with its binding site enhances proton binding. Modelling further suggests that protonated channels are capable of opening but with a lower open probability than unprotonated channels. These data and analyses are consistent with $Zn^{2+}$-mediated inhibition of NMDA receptors primarily reflecting enhancement of proton inhibition.**

(Received 27 August 2007; accepted after revision 23 November 2007; first published online 29 November 2007)
**Corresponding author** S. F. Traynelis: Department of Pharmacology, Emory University School of Medicine, Rollins Research Center, Atlanta, GA 30322, USA. Email: strayne@emory.edu

The NMDA subtype of glutamate receptor ion channels is a non-selective cation channel with high calcium permeability that has been implicated as playing a critical role in both physiological and pathophysiological processes. NMDA receptor function has been demonstrated to be regulated by both intracellular modulators, such as kinases and scaffolding proteins, and extracellular modulators including redox agents and various ions (Dingledine *et al.* 1999; Erreger *et al.* 2004). Two such extracellular modulators whose range of activity probably falls within the concentrations present during physiological and/or pathological conditions are zinc ions ($Zn^{2+}$) and protons (pH).

$Zn^{2+}$ has been demonstrated to be localized in synaptic vesicles at glutamatergic presynaptic terminals (Salazar *et al.* 2005) and has been suggested to be released in an activity-dependent manner, making it an important potential modulator of glutamate receptor function (Smart *et al.* 2004). However, a wide range of values have been suggested for $Zn^{2+}$ concentrations in the synaptic cleft following glutamate release, and thus the quantity of $Zn^{2+}$ released from presynaptic terminals remains controversial (Ueno *et al.* 2002; Kay, 2003; Frederickson *et al.* 2006).

NMDA receptors containing the NR2A subunit exhibit high affinity voltage-independent inhibition by $Zn^{2+}$ (Williams, 1996; Chen *et al.* 1997; Paoletti *et al.* 1997). The molecular determinants of high affinity zinc binding have been demonstrated to lie in the amino terminal domain of the NR2A subunit (Choi & Lipton, 1999; Low *et al.* 2000; Paoletti *et al.* 2000; Hatton & Paoletti, 2005). The extracellular amino terminal domain is present in all ionotropic glutamate receptors, and is thought to adopt a clamshell-like organization with some homology to bacterial amino acid binding proteins. $Zn^{2+}$ binding to NR2A and polyamine binding to NR2B are the only known native ligands for the amino terminal domain (Masuko *et al.* 1999; Paoletti *et al.* 2000), although ifenprodil and its analogues are synthetic molecules that bind selectively to the NR2B amino terminal domain (Perin-Dureau *et al.* 2002; Wong *et al.* 2005). The amino terminal domain has also been suggested to play a role in subunit dimerization and receptor assembly (Leuschner & Hoch, 1999; Ayalon & Stern-Bach, 2001; Meddows *et al.* 2001; Ayalon *et al.* 2005).

Extracellular proton concentration (commonly expressed as $pH = -\log_{10}[H^+]$) is normally kept under

This paper has online supplemental material.

 DOI: 10.1113/jphysiol.2007.143941

tight physiological control (Chesler, 2003). However, the inside of glutamatergic synaptic vesicles has an exceptionally high proton concentration (pH 5.7) (Miesenbock *et al.* 1998), suggesting that vesicle release under conditions of high activity might be capable of acidifying the local extracellular environment and modifying synaptic NMDA receptor function through a pH-dependent mechanism (DeVries, 2001). In addition, activity-dependent alkalinization of the extracellular space can also influence NMDA receptor response amplitudes (Gottfried & Chesler, 1994; Makani & Chesler, 2007). NMDA receptor overactivation mediates some forms of excitotoxicity, and proton inhibition has been proposed to be one endogenous neuroprotective mechanism to attenuate NMDA receptor activation in ischaemic conditions associated with acidification and high levels of glutamate release (Tombaugh & Sapolsky, 1993). Protons inhibit NMDA receptors in a voltage-independent manner with an $IC_{50}$ within the physiological range: 30–120 nM $H^+$ for NR1/NR2A (Low *et al.* 2000). Extensive site-directed mutagenesis throughout both NR1 and NR2 subunits has implicated a highly conserved region among glutamate receptors at the extracellular end of the second transmembrane domain (and excluded other parts of the protein) as an important determinant of proton inhibition (Low *et al.* 2003). This region contains the residue at which the 'lurcher' mutation was originally identified in the D-serine-binding $\delta 2$ glutamate receptor subunit (Naur *et al.* 2007). Mutation of this residue in $\delta 2$, GluR1, GluR6 or NR1 results in either constitutive activation in the absence of agonist or in greatly increased apparent agonist affinity, suggesting a critical role for this region in channel gating (Kohda *et al.* 2000; Taverna *et al.* 2000; Klein & Howe, 2004; Vogel *et al.* 2006).

Zinc and proton inhibition are recognized to share common structural determinants (Traynelis *et al.* 1998). Multiple lines of evidence have suggested that high affinity $Zn^{2+}$ inhibition acts through enhancing sensitivity of NMDA receptors to inhibition by extracellular protons (Choi & Lipton, 1999; Low *et al.* 2000; Zheng *et al.* 2001; Erreger & Traynelis, 2005). That is, binding of zinc has been proposed to shift the sensitivity (p*K*a) of the proton sensor such that protonation is enhanced at physiological pH. Consistent with this hypothesis, we report here that $Zn^{2+}$ and protons similarly modulate single-channel activity of recombinant NR1/NR2A by both reducing mean channel open time and reducing channel open probability. Kinetic analysis of single-channel recordings suggests that $Zn^{2+}$ inhibition reflects enhancement of proton sensitivity.

## Methods

Human embryonic kidney 293 (HEK293) cells were maintained and transiently transfected by the calcium phosphate method with cDNA encoding NR1-1a (GenBank accession numbers U11418 and U08261; pCIneo vector; hereafter called NR1), NR2A (D13211; pCIneo), and green fluorescent protein at a ratio of 1 : 2 : 1 (0.2 $\mu$g ml$^{-1}$ NR1) for 4–12 h, as previously described (Zheng *et al.* 1998). Currents from outside-out patches were digitally recorded with pClamp8 software using an Axopatch 200B amplifier (Molecular Devices, Union City, CA, USA). Single-channel records were filtered at 5 kHz using an eight-pole Bessel filter (−3 dB; Frequency Devices, Haverhill, MA, USA) and digitized at 40 kHz. Thick-walled borosilicate glass (1.5 mm outer diameter; 0.85 mm inner diameter; Warner Instruments) was fire polished to a resistance of 6–9 MΩ, and Sylgard (Dow Corning, Midland, MI, USA) was applied to the pipette tip. The extracellular solution consisted of (mM): 150 NaCl, 10 Hepes, 10 tricine, 0.5 $CaCl_2$, 3 KCl with 50 $\mu$M glycine and 1 mM glutamate (pH 7.3, 23°C). For some experiments, pH was adjusted to 6.7 by addition of HCl. The internal solution consisted of (mM): 110 caesium gluconate, 30 CsCl, 5 Hepes, 4 NaCl, 0.5 $CaCl_2$, 2 $MgCl_2$, 5 BAPTA, 2 Na-ATP and 0.3 Na-GTP (pH 7.35). Tricine-buffered $Zn^{2+}$ solutions were prepared using a binding constant of $10^{-5}$ M with WINMAX software (http://www.stanford.edu/~cpatton/maxc.html). The tricine concentration was 10 mM and the total $Zn^{2+}$ concentration was 27 $\mu$M, which gives a free $Zn^{2+}$ concentration of 300 nM. Free proton concentrations were calculated with an activity coefficient of 0.8. No voltage correction was applied for the junction potential.

Records were idealized with a segmental k-means algorithm (Qin, 2004) using QuB software (www.qub.buffalo.edu). Use of 0.5 mM extracellular $Ca^{2+}$ decreased the frequency of lower subconductance level openings. All conductance levels were assumed to be equal for the analysis. In order to segment data into bursts, we calculated a critical shut time ($T_{crit}$) that would separate the three fastest shut time components from longer closed times. We calculated $T_{crit}$ to minimize the total number of misclassified events (Jackson *et al.* 1983; Colquhoun & Sigworth, 1995; Erreger *et al.* 2005*a*). $T_{crit}$ values for NR1/NR2A channel records shown in Fig. 1 were 32 ms for control conditions (< 1% events misclassified) and 37 ms for recordings made in the presence of 300 nM $Zn^{2+}$ (3% of events misclassified). As these values are virtually indistinguishable from the $T_{crit}$ value of 30 ms used in previous studies of NR1/NR2A channels (Erreger *et al.* 2005*a*,*b*), we used 30 ms to identify bursts here to allow more direct comparison of our analyses with these previous results. Bursts with multiple channels simultaneously open were not analysed. Dwell-time histograms were generated and fitted using Channelab (www.synaptosoft.com) with an imposed dead time of 50 $\mu$s. Maximal interval likelihood fitting (MIL; Qin *et al.* 1996) was performed with an imposed dead time of 50 $\mu$s using QuB software; similar results

were obtained when a dead time of 100 $\mu$s was imposed (data not shown).

For patches with no double openings, the control period was analysed with the following equation (Colquhoun & Hawkes, 1995):

$$P = [(1 - P_{ON})/(1 - P_{ON}/2)]^{n-1} \quad (1)$$

$P$ is the probability of the number of observed single openings before observing a double opening in a patch with two channels. $P_{ON}$ is the observed probability of being open in the experimental record; $n$ is the number of single openings observed. We are aware that the burst structure of NR2A openings is not ideal for using this approximation to determine the number of channels in a patch. We therefore re-analysed the data based on the probability of the observed number of bursts before observing overlapping bursts in a patch with two channels (Colquhoun & Hawkes, 1995). Similar results are found with this alternate

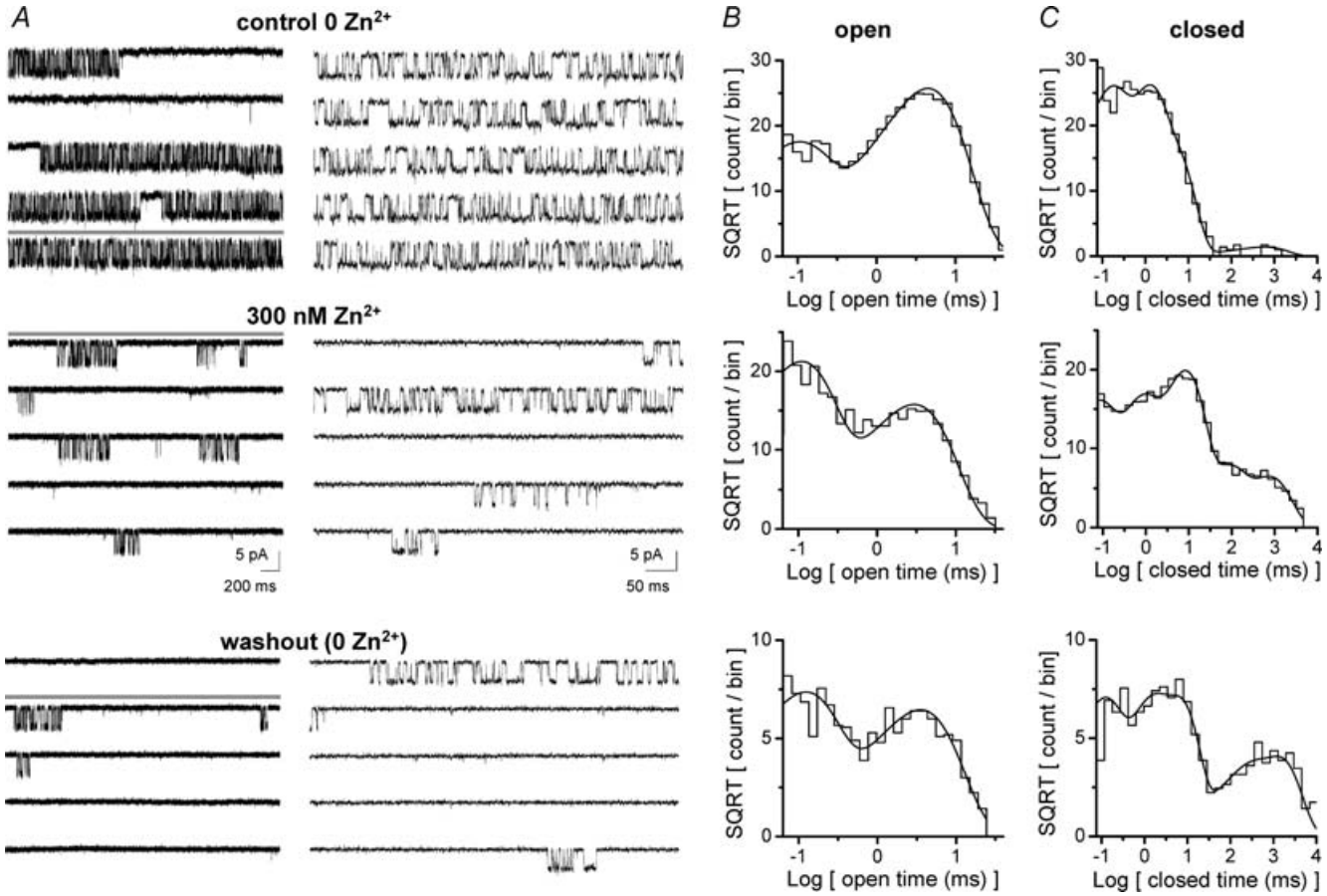


**Figure 1. $Zn^{2+}$ alters the kinetic properties of recombinant NR1/NR2A channels in outside-out patches from HEK293 cells**

*A*, outside-out patches were exposed to 1 mM glutamate and 50 $\mu$M glycine under control (0 $Zn^{2+}$, 10 mM tricine), zinc (300 nM free $Zn^{2+}$ buffered by 10 mM tricine), and washout (0 $Zn^{2+}$, 10 mM tricine; not shown). The holding potential was −80 mV. Currents were sampled at 40 kHz and filtered at 5 kHz for analysis, but are sampled at 5 kHz and filtered at 2 kHz for display. Representative current traces from a patch with only a single active channel are displayed on two different time scales for each condition; downward deflections reflect channel openings. The thick grey line on the left trace indicates the portion displayed at a higher time resolution in the right trace. *B* and *C*, the distribution of open (*B*) and closed (*C*) duration dwell times is plotted for each condition for the same patch as panel *A*. The open dwell time distribution from this patch was fitted by the sum of two exponential components with time constants and relative amplitudes of $\tau$1 0.09 ms (29%), $\tau$2 4.5 ms (71%) for control; $\tau$1 0.10 ms (63%), $\tau$2 3.0 ms (37%) for 300 nM $Zn^{2+}$; $\tau$1 0.12 (55%), $\tau$2 3.5 ms (45%) for washout. The closed dwell time distribution was fitted by the sum of four or five exponential components with time constants and relative amplitudes of $\tau$1 0.13 ms (37%), $\tau$2 1.0 ms (40%), $\tau$3 4.0 ms (22%), $\tau$4 590 ms (1%) for control; $\tau$1 0.07 ms (23%), $\tau$2 0.63 ms (22%), $\tau$3 8.0 ms (44%), $\tau$4 72 ms (6%), $\tau$5 720 ms (5%) for 300 nM $Zn^{2+}$; and $\tau$1 0.10 ms (28%), $\tau$2 1.0 ms (19%), $\tau$3 6.0 ms (35%), $\tau$4 210 ms (5%), $\tau$5 1300 ms (13%) for washout. We recorded 7901 openings under the control condition, 5098 openings in the presence of 300 nM $Zn^{2+}$, and 790 openings following washout of $Zn^{2+}$ from this patch.

analysis, which also suggests these patches contain a single active channel.

The distribution of lengths of open periods adjacent to closed times within a specified range was determined. Conditional open duration distributions were constructed from either the preceding or following opening adjacent to a closed time of a specified length. Identical results were obtained from openings preceding or following closed periods, as expected if the channel obeys the law of microscopic reversibility. The closed duration intervals used to define the conditional open durations were chosen from critical times calculated to minimize the total number of misclassified events (Jackson *et al.* 1983) in the fitted shut time distribution obtained from uninterrupted recordings of NR1/NR2A channel activity in response to supra-maximal co-agonist concentrations from a patch that contained only one active channel (see Fig. 1). In addition, the runs test was applied to apparent single-channel open durations as previously described (Colquhoun & Sakmann, 1985; Colquhoun & Sigworth, 1995) using a critical open time of 0.5 ms.

Statistical analysis was performed in Prism 3 (Graphpad, San Diego, CA, USA). Student's *t* test was employed for single comparisons and ANOVA with Tukey's *post hoc* test was employed for multiple comparisons. All data are expressed as mean ± S.E.M.

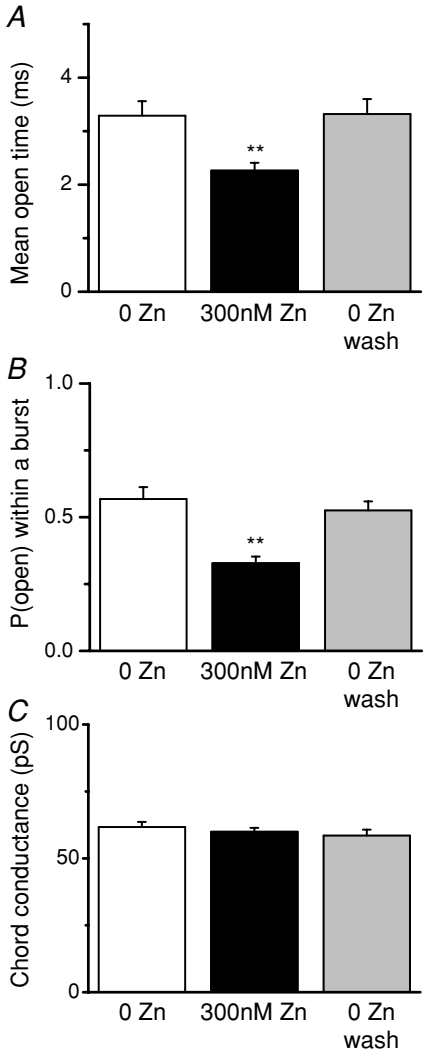


**Figure 2. $Zn^{2+}$ decreases the mean channel open time and open probability within a burst but does not alter the single-channel current amplitude**

*A*, the mean channel open time is reversibly decreased by 300 nM extracellular $Zn^{2+}$ from 3.3 ± 0.3 to 2.3 ± 0.2 ms ($n = 7$). *B*, the open channel probability within a burst is reversibly decreased by $Zn^{2+}$ from 0.57 ± 0.04 to 0.33 ± 0.02 ($n = 7$); burst or individual activations were identified with a 30 ms critical time (see Methods). *C*, the chord conductance determined at −80 mV is not altered by extracellular $Zn^{2+}$ ($n = 7$). $^{**}P < 0.01$, repeated-measures ANOVA with Tukey's *post hoc* test.

## Results

### Inhibition of NR1/NR2A channels by extracellular $Zn^{2+}$

Recombinant NR1 and NR2A NMDA receptor subunits were transiently transfected into HEK293 cells. Patch clamp recording was performed in the outside-out patch configuration with a maximally effective concentration of glycine (50 μM) and glutamate (1 mM) at a voltage of −80 mV. Typically, control data (0 $Zn^{2+}$, 10 mM tricine, pH 7.3) were collected for 5 min, followed by 5 min in the presence of 300 nM free $Zn^{2+}$ (buffered by 10 mM tricine), and finally a washout back to the control condition for 5 min. A concentration of 300 nM $Zn^{2+}$ was chosen to saturate the high affinity inhibition ($IC_{50} \approx 30$ nM) (Williams, 1996; Chen *et al.* 1997; Paoletti *et al.* 1997; Choi & Lipton, 1999; Low *et al.* 2000; Zheng *et al.* 2001) but not induce low affinity voltage-dependent channel block ($IC_{50} \approx 30$ μM) (Williams, 1996; Chen *et al.* 1997; Paoletti *et al.* 1997). Of seven patches that met our criteria for analysis, two patches exhibited no double channel openings over the course of the 15 min of recording. Based on a simple approximation of the probability of observing a given number of single openings from a patch that actually contained two channels (see Methods), we calculate this probability as $P < 0.001$ for the control period of each of these two patches, suggesting that they probably contain a single functional channel. One of these patches with 7901 channel opening events without any double channel openings during the control period is shown in Fig. 1. The open time distribution was fitted with the sum of two exponential components (Fig. 1*B*). The distribution of closed times was complex, and could be fitted with at least four exponential components (Fig. 1*C*). While the overall channel open probability runs down over the course of the recording, as manifested by increasing frequency of long closed times, channel properties within a burst of channel openings are identical for the initial control period compared to the washout (see Figs 2, 3 and 7 below).

For all patches, the data were segmented into bursts based on a critical shut time of 30 ms as a burst terminator (Erreger *et al.* 2005*a*). Functional channel properties within a burst were then determined (Fig. 2). The similarity in results from patches that probably contain a single channel and patches with multiple channels supports our choice of 30 ms for a critical shut time for burst identification. The presence of 300 nM $Zn^{2+}$ caused a significant $30 \pm 3\%$ reduction in the mean channel open time ($P < 0.01$; $n = 7$; ANOVA; Fig. 2*A*) as well as a $40 \pm 5\%$ reduction in open probability within a burst ($P < 0.01$; $n = 7$; ANOVA; Fig. 2*B*). The open probability was calculated as the fraction of time in the open state for all events for each patch after segmentation into bursts, and was 0.55 under control conditions, consistent with previous reports (Erreger *et al.* 2005*a*). The effects of extracellular $Zn^{2+}$ on mean open time and on open probability were completely reversed upon washout of $Zn^{2+}$. NR1/NR2A receptors primarily open to a single conductance level of ~60 pS in the presence of 0.5 mM extracellular free $Ca^{2+}$ (Fig. 2*C*). $Zn^{2+}$ (300 nM) had no effect on the single-channel chord conductance at −80 mV.

The composite distribution of channel open durations pooled from all patches could be best fitted with two exponential components (Fig. 3*A*). Open time distributions from individual patches were also fitted with two exponential components (Fig. 3*B–D*). The time constant for the shorter component ($\tau 1$) was unchanged by 300 nM $Zn^{2+}$ (Fig. 3*B*). By contrast, 300 nM $Zn^{2+}$ reversibly decreased the time constant for the longer component ($\tau 2$; Fig. 3*C*). In addition, the relative area of $\tau 1$ in the distribution was reversibly increased by $Zn^{2+}$ (Fig. 3*D*). The shift in the open time suggests that $Zn^{2+}$-bound receptors retain the ability to open, consistent with the incomplete inhibition by saturating $Zn^{2+}$ (Paoletti *et al.* 1997; Low *et al.* 2000; Erreger & Traynelis, 2005; Hatton & Paoletti, 2005).

Correlations between the lengths of an open time and an adjacent closed time can provide information about the mechanism of channel activation. Correlations between the duration of open and closed times have previously been described for recombinant NR1/NR2A receptors recorded in outside-out patches excised from *Xenopus laevis* as well as native NMDA receptors in CA1

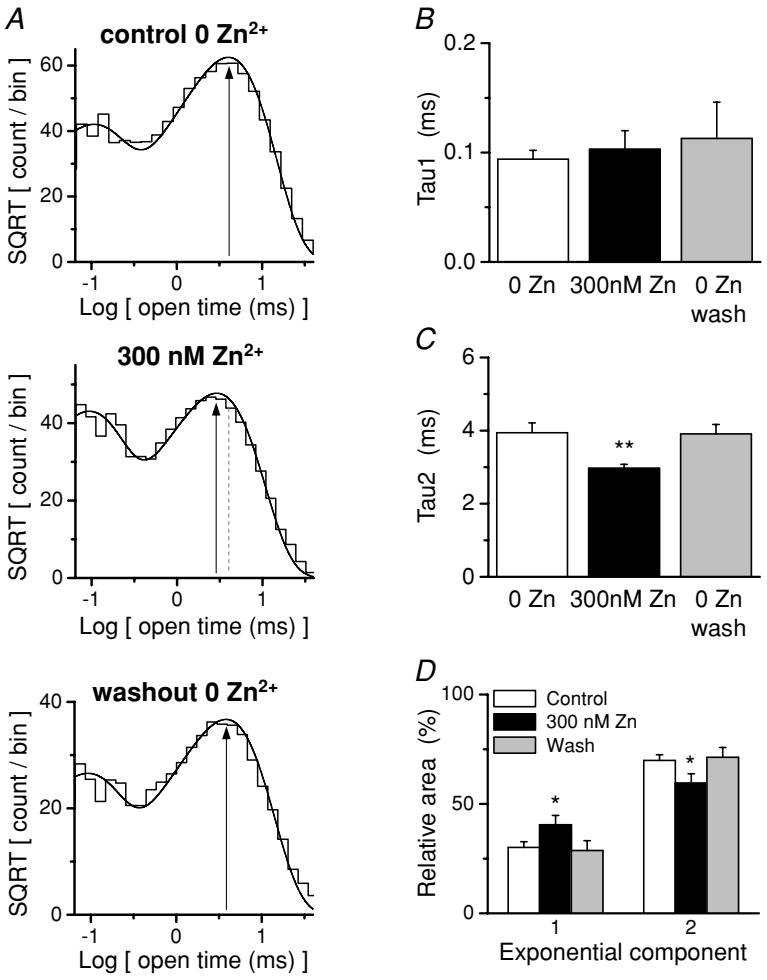


**Figure 3. $Zn^{2+}$ alters the distribution of open channel dwell durations**
*A*, the distribution of open times for each condition pooled among all 7 patches is shown. Vertical lines indicate the second fitted time constant, which is accelerated by 300 nM extracellular $Zn^{2+}$. *B*, the mean of the briefer open time constant from fits to individual patches is displayed for all conditions. *C*, the mean of the longer fitted open time constant is displayed for the various conditions. *D*, the effect of $Zn^{2+}$ on the mean relative amplitude of each time constant is summarized. For all panels $n = 7$. $^*P < 0.05$ and $^{**}P < 0.01$, repeated-measures ANOVA with Tukey's *post hoc* test.

pyramidal cells (Gibb & Colquhoun, 1991; Schorge *et al.* 2005; Wyllie *et al.* 2006). However, Zhou & Auerbach (2005) did not observe correlations in cell-attached patch recordings of NR1/NR2A receptors in response to maximal concentrations of co-agonists. To evaluate whether correlations existed in our data set and to evaluate the effect of extracellular $Zn^{2+}$ on potential correlations, we first performed a runs test for correlations among open times in patches that contain only one active channel using a critical open time of 0.5 ms (Colquhoun & Sigworth, 1995). This analysis yielded strong support of runs of short and long duration openings for recordings both in control conditions and in the presence of 300 nM $Zn^{2+}$ with the $z$ statistic ranging between −8.1 and −17.7.

We subsequently constructed conditional distributions of adjacent intervals to examine the strength of any correlations in the data record. Figure 4*A* shows conditional distributions of apparent intra-burst open times adjacent to brief (0.05–0.27 ms) or prolonged (2.65–32.6 ms) intra-burst closed times. The distribution of open times adjacent to brief closed times shows similar fitted time constants as the distribution of open times adjacent to prolonged closures, but an increase in the area of the slower component. This trend could be seen in the analysis of the mean open time adjacent to closed times in a specified range. We constructed this relationship for intra-burst open times determined from all patch recordings, as well as from all open times in two patches

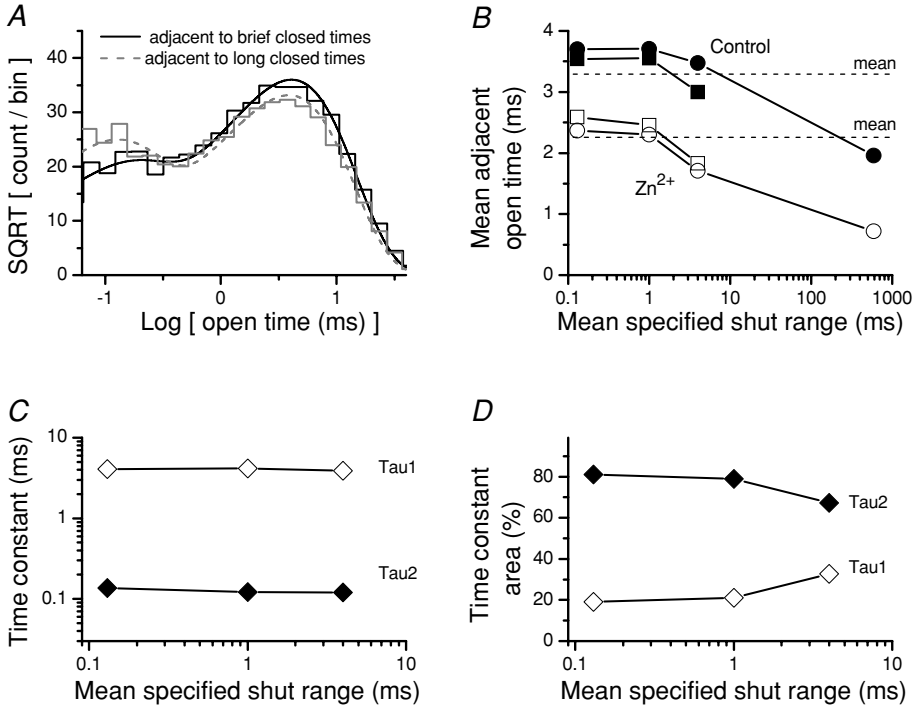


**Figure 4. Correlations between open and closed durations of NR1/NR2A channels in outside-out patches from HEK293 cells**

*A*, the closed time histogram from a patch with a single active channel recorded in response to maximal concentrations of agonist (Fig. 1) was used to determine critical closed times to separate the four fitted shut time components as described in the Methods (Jackson *et al.* 1983). Critical times were 0.27, 2.65 and 32.6 ms. Conditional distributions were constructed from pooled data from all patches for intra-burst apparent open durations adjacent to a brief closed durations in the range of 0.05–0.27 ms (continuous black line) or adjacent to longer duration closed times in the range of 2.65–32.6 ms (broken grey line). The distributions and respective fitted exponential components for openings adjacent to brief closures were scaled to contain the same number of events as distributions for open times adjacent to long closed times. *B*, the mean of conditional apparent intra-burst open durations (squares) pooled from all patches recorded in control conditions or in 300 nM $Zn^{2+}$ are plotted against the fitted time constants describing the closed time distribution (Fig. 1). The mean apparent open times determined from two patches that contained one active channel are shown as circles. The critical times defining each closed duration range were determined from the histogram in Fig. 1*C*, and were (in ms) 0.05–0.27, 0.27–2.65, 2.65–32.6 and 32.6–10 000. The dashed lines show the mean intra-burst open durations. *C*, the fitted time constants of exponential components describing the conditional open duration distributions for recordings in the absence of $Zn^{2+}$ are shown. Fitted intra-burst time constants were (for $\tau 1$) 0.14, 0.12 and 0.12 ms and (for $\tau 2$) 4.1, 4.2 and 3.9 ms. *D*, the areas of the two time constants from the fitted conditional distributions are shown, and were (for $\tau 1$) 19, 21 and 33% and (for $\tau 2$) 81, 79 and 67%.

that appear to contain a single active channel (Fig. 4*B*). As previously reported for recordings in outside-out patches (Gibb & Colquhoun, 1991; Schorge *et al.* 2005; Wyllie *et al.* 2006), this analysis showed a negative correlation, in that on average open times adjacent to longer closed times were shorter. The magnitude was similar to previous reports. Importantly, the correlations persisted in the presence of saturating concentration of extracellular $Zn^{2+}$. Evaluation of the fitted time constants to the conditional open time distributions showed the change in mean open time reflected a change in the area of fitted time constants rather than any change in either time constant (Fig. 4*C* and *D*).

### Inhibition of NR1/NR2A channels by extracellular protons

Previous studies have demonstrated a functional link between the inhibition of NR1/NR2A NMDA receptors by $Zn^{2+}$ and protons (Choi & Lipton, 1999; Low *et al.* 2000). We therefore examined the effects of reduced pH (increased proton concentration) on NR1/NR2A single-channel properties. We selected a proton concentration (250 nM $H^+$, pH 6.7) that was known to cause a similar level of steady-state inhibition at the macroscopic level as a saturating $Zn^{2+}$ concentration (~60% inhibition) when compared to the control condition (62 nM $H^+$, pH 7.3; Low *et al.* 2000). If extracellular $Zn^{2+}$ acts through enhancement of proton inhibition, we predict that this concentration of protons should have similar effects on single-channel properties as $Zn^{2+}$. Figure 5*A* shows a representative recording from an outside-out patch at pH 7.3 and pH 6.7. Open time histograms in this patch could be fitted by the sum of two exponential components. Similar to the effects of 300 nM $Zn^{2+}$, increasing the extracellular $H^+$ concentration accelerated the second time constant in this patch (Fig. 5*B*).

We subsequently analysed data from five patches in which we recorded both at pH 7.3 and 6.7. Increasing the proton concentration to 250 nM (pH 6.7) significantly decreased mean channel open time from $3.0 \pm 0.2$ to $1.4 \pm 0.1$ ms (Fig. 5*C*). Reduced pH also decreased the open probability within a burst from $0.64 \pm 0.03$ to $0.30 \pm 0.03$ (Fig. 5*D*), consistent with the effects of 300 nM extracellular $Zn^{2+}$. In addition, reduced extracellular pH did not alter the main unitary channel conductance level recorded from NR1/NR2A receptors in the presence of 0.5 mM $Ca^{2+}$, again consistent with the effects of

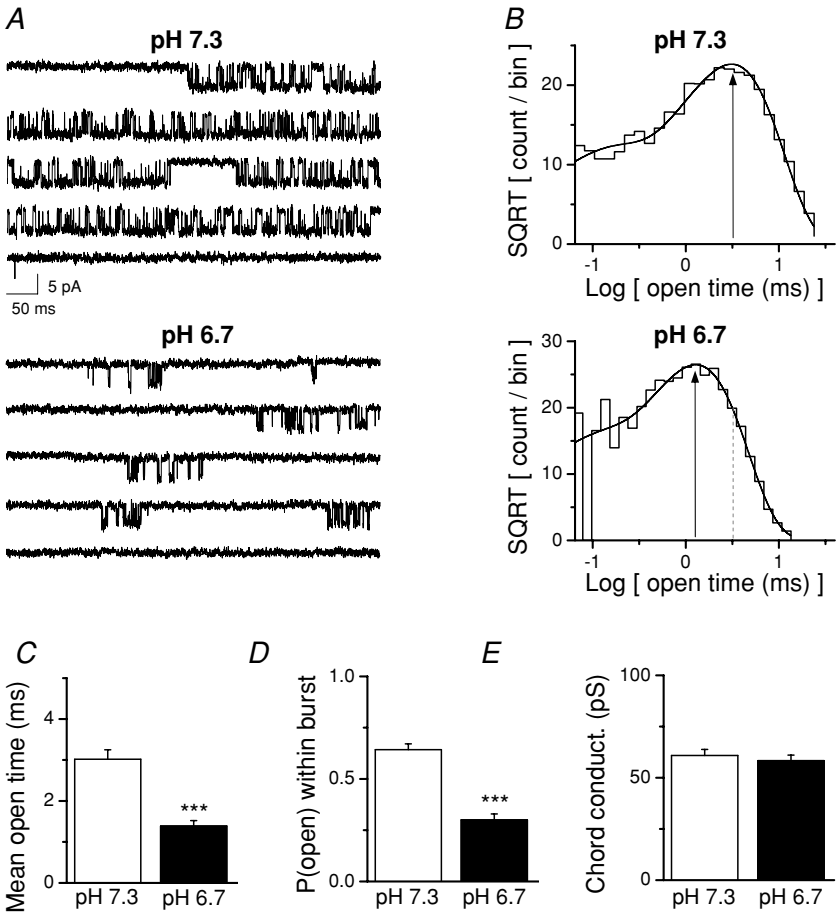


**Figure 5. Increased proton concentration reduces the open probability of NR1/NR2A channels in outside-out patches**
*A*, representative current traces from the same patch are shown at two different extracellular pH values. *B*, the distribution of open dwell times is plotted for each pH for the same patch shown in panel *A*. The open dwell time distribution was fitted by the sum of two exponential components with time constants and relative amplitudes of $\tau 1$ 0.11 ms (15%), $\tau 2$ 3.1 ms (85%) for control pH 7.3 and time constants of $\tau 1$ 0.07 ms (15%), $\tau 2$ 1.3 ms (85%) for pH 6.7. Vertical lines show the second fitted time constant. 6140 openings were recorded at pH 7.3 and 8889 openings at pH 6.7. *C*, the mean channel open time ($n = 5$ patches) was decreased in low pH. *D*, the mean open channel probability within a burst was also decreased by low pH ($n = 5$). *E*, the chord conductance at −80 mV was not altered by low pH ($n = 5$). For all panels, $^{***}P < 0.001$, paired *t* test.

$Zn^{2+}$ (Fig. 5*E*). Figure 6 shows that the effect of pH on the distribution of open times pooled from all five patches is similar to the effect of 300 nM $Zn^{2+}$ (compare with Fig. 3). That is, increased proton concentration decreased the time constant for the longer open time component ($\tau 2$). Thus, the effects of proton inhibition on single-channel currents recorded in outside-out patches largely mirror properties of $Zn^{2+}$ inhibition on recombinant NR1/NR2A. These data are consistent with the hypothesis that $Zn^{2+}$ binding enhances proton inhibition.

### Kinetic analysis of $Zn^{2+}$ inhibition of NR1/NR2A channels

In order to gain some mechanistic insight into the effects of $Zn^{2+}$ on NR1/NR2A receptor gating, we fitted the sequence of single-channel openings and closings for each patch with explicit models of channel function using maximum interval likelihood fitting (MIL, see Methods; Fig. 7*A* and *B*). Data were fitted by two models, a linear model (Scheme I) and a cyclic gating model (Scheme II), both of which were based on previously published models of NMDA receptor function (Popescu & Auerbach, 2003; Popescu *et al.* 2004; Erreger *et al.* 2005*a*,*b*; Schorge *et al.* 2005; Zhou & Auerbach, 2005). Two explicit open states were included and were assumed to be interconnected in the models (Popescu & Auerbach, 2003; Zhou & Auerbach, 2005). All states are fully liganded as all data fitted were in the presence of saturating agonist concentrations. Scheme I represents sequential conformational changes leading to gating (Popescu & Auerbach, 2003; Popescu *et al.* 2004; Zhou & Auerbach, 2005) and Scheme II represents an independent two-step gating model in which the receptor undergoes separate conformational changes required for gating in any order (Banke & Traynelis, 2003; Erreger *et al.* 2005*a*,*b*; Schorge *et al.* 2005). The models are not equivalent because the first open state encountered has different connectivity. The effect of $Zn^{2+}$ on the fitted rate constants for each transition in both models is displayed in Fig. 7*C* and *D*. The mean rate constants averaged across all patches are given in Table 1. Average rates were virtually identical to the rates derived from global fitting of the pooled data from all patches. Extracellular $Zn^{2+}$ significantly altered only the reverse rate of the slowest transition preceding channel opening ($k_2$) in both models. This is the analogous transition that is modified by partial agonists acting at the glutamate binding site (Erreger *et al.* 2005*b*) and the analogous rate that controls the main difference in gating between NR1/NR2A and NR1/NR2B receptors (Erreger *et al.* 2005*a*). Whereas the experimentally determined mean open time was reduced by 300 nM extracellular $Zn^{2+}$, none of the average rates into or out of the open states in the model were statistically significantly different based on fits to individual patches. However, there was a clear increase in the closing rate ($k_4$) from the briefer gateway open state derived from the global fit of the pooled data (Table 1). The mean open times predicted from Schemes I and II changed from 2.9 and 3.1 ms in control to 1.9 and 1.9 ms in 300 nM $Zn^{2+}$, respectively. The change in $k_2$ is consistent with a $Zn^{2+}$-induced reduction in the open probability, since the reverse of the initial pre-gating step in this model is accelerated in $Zn^{2+}$-bound receptors. As expected, the open probability was reduced for Schemes I and II from 0.56 and 0.61 in control to 0.30 and 0.29 in 300 nM

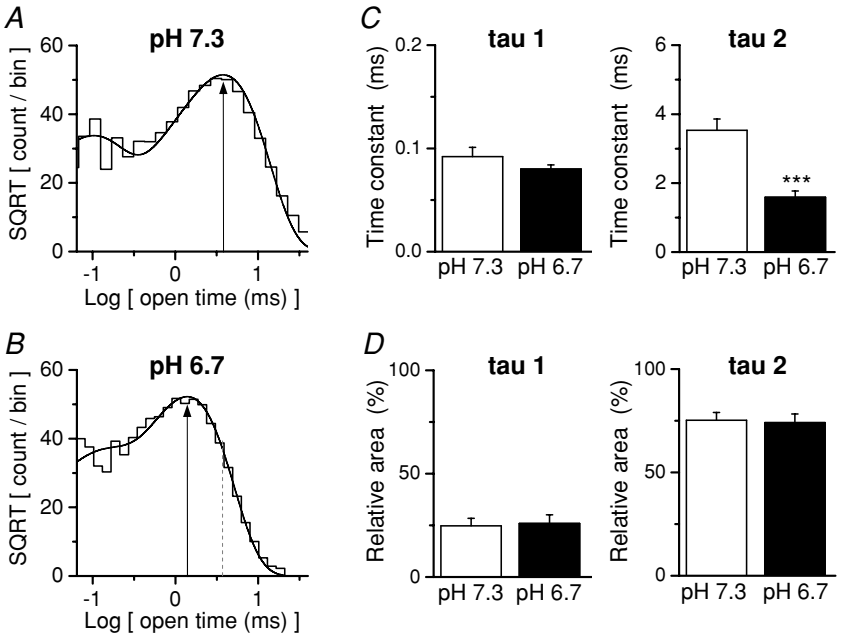


**Figure 6. Increased proton concentration alters the distribution of open channel dwell durations**
*A* and *B*, the distribution of open times pooled among all 5 patches is shown at pH 7.3 (*A*) and pH 6.7 (*B*). 27 613 openings were recorded at pH 7.3 and 34 327 openings at pH 6.7. *C*, the mean fitted time constants for the open time distribution are displayed ($n = 5$). *D*, the mean relative areas for the fitted time constants for all five patches are shown. $^{***}P < 0.001$, paired *t* test.

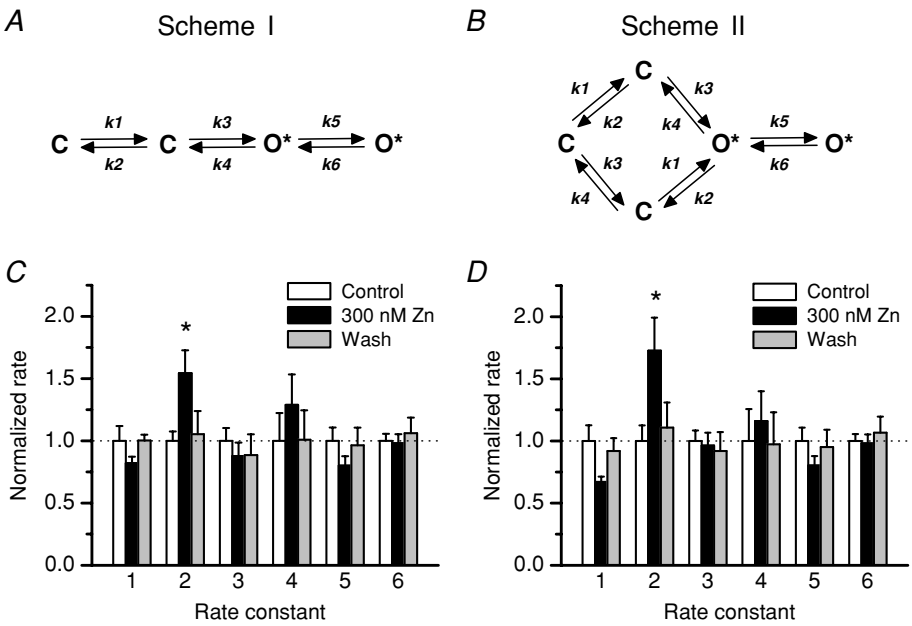


**Figure 7. Maximum interval likelihood fitting of $Zn^{2+}$ and pH modulation of channel activity**
Recordings were performed in the presence of a saturating concentration of agonist and divided into segments to remove desensitization. Therefore explicit agonist binding and desensitization rates are not included in the models. *A*, Scheme I is a simplified model of gating with two sequential gating steps. In this scheme, 'C' represents closed non-conducting states and 'O*' represents open conducting state. *B*, Scheme II is a model with two independent gating steps connected in a manner to allow them to open in either order. This model has previously been suggested to represent a slow NR2-dependent step ($k_1/k_2$) and a fast NR1-dependent step ($k_3/k_4$) (Banke & Traynelis, 2003). *C* and *D*, each rate constant was normalized to the mean value of the control condition for all 7 patches in the $Zn^{2+}$ data set. The raw values for the rate constants are given in Table 1. *$P < 0.05$, repeated-measures ANOVA with Tukey's *post hoc* test.

**Table 1. Idealized and segmented current records from the same patches were fitted with the models shown in Fig. 7*A* and *B***

| | Control | | | 300 nM $Zn^{2+}$ | | | Washout | | |
|---|---|---|---|---|---|---|---|---|---|
| | Mean | S.E.M. | Global fit | Mean | S.E.M. | Global fit | Mean | S.E.M. | Global fit |
| Scheme I | | | | | | | | | |
| $k_1$ | 460 | 55 | 430 | 380 | 28 | 380 | 460 | 29 | 450 |
| $k_2$ | 1500 | 120 | 1400 | 2200 | 310 | 2300 | 1600 | 370 | 1600 |
| $k_3$ | 2400 | 250 | 2300 | 2000 | 290 | 1900 | 2100 | 530 | 2100 |
| $k_4$ | 3800 | 840 | 2900 | 4600 | 1100 | 5000 | 3800 | 1200 | 3900 |
| $k_5$ | 6500 | 700 | 6300 | 5100 | 560 | 5800 | 6200 | 1200 | 7200 |
| $k_6$ | 880 | 50 | 910 | 880 | 70 | 820 | 930 | 140 | 830 |
| logL/event | 5.13 | — | 5.11 | 5.01 | — | 4.99 | 4.99 | — | 5.05 |
| Scheme II | | | | | | | | | |
| $k_1$ | 300 | 38 | 280 | 200 | 13 | 210 | 280 | 31 | 280 |
| $k_2$ | 880 | 110 | 760 | 1500 | 240 | 1600 | 980 | 180 | 1100 |
| $k_3$ | 3200 | 260 | 3000 | 3000 | 330 | 2800 | 2900 | 480 | 2800 |
| $k_4$ | 2900 | 730 | 2200 | 3300 | 690 | 3400 | 2800 | 740 | 2900 |
| $k_5$ | 6500 | 690 | 6300 | 5200 | 480 | 5800 | 6100 | 900 | 7200 |
| $k_6$ | 880 | 49 | 900 | 880 | 69 | 820 | 940 | 110 | 830 |
| logL/event | 5.12 | — | 5.11 | 5.01 | — | 4.99 | 4.99 | — | 5.05 |

All rates have units of $s^{-1}$. Data from each patch were fitted independently and the mean values and standard errors are shown ($n = 7$). Additionally, records from all 7 patches were pooled and fitted simultaneously with the result given as the global fit. The total number of openings was 43 526 for control, 31 200 for $Zn^{2+}$, and 16 384 for washout. Rate constants are given to two significant digits. For all tables, the logarithm of the maximum likelihood determined during MIL fitting is given normalized to the number of channel dwell times (logL/event).

$Zn^{2+}$, respectively. These changes are consistent with our single-channel data (Fig. 2).

### $Zn^{2+}$ enhances proton sensitivity of NR1/NR2A single channels

The kinetic analysis described in Fig. 7 suggests that $Zn^{2+}$ binding to NR2A changes the rates of specific gating steps, rather than causing a global modification of all aspects of receptor function. However, this model does not take into account previous data (Choi & Lipton, 1999; Low *et al.* 2000; Erreger & Traynelis, 2005) suggesting that $Zn^{2+}$ binding to the NR2A amino terminal domain enhances inhibition by extracellular protons. The binding of two different ions ($Zn^{2+}$ and protons) to a complex gating scheme provides a myriad of potential models to consider (see for example Banke *et al.* 2005). Rather than fitting all possible kinetic schemes that include individual proton and $Zn^{2+}$ binding steps as well as a full reaction scheme, we focused on progressively expanding the linear model shown in Scheme I (Fig. 7) by adding a protonated arm. We used a series of related models to explore how variation of the states that could be protonated, variation of open probability of protonated states, and conservation of rates between protonated and unprotonated arms impacted the ability of the models to reproduce our data.

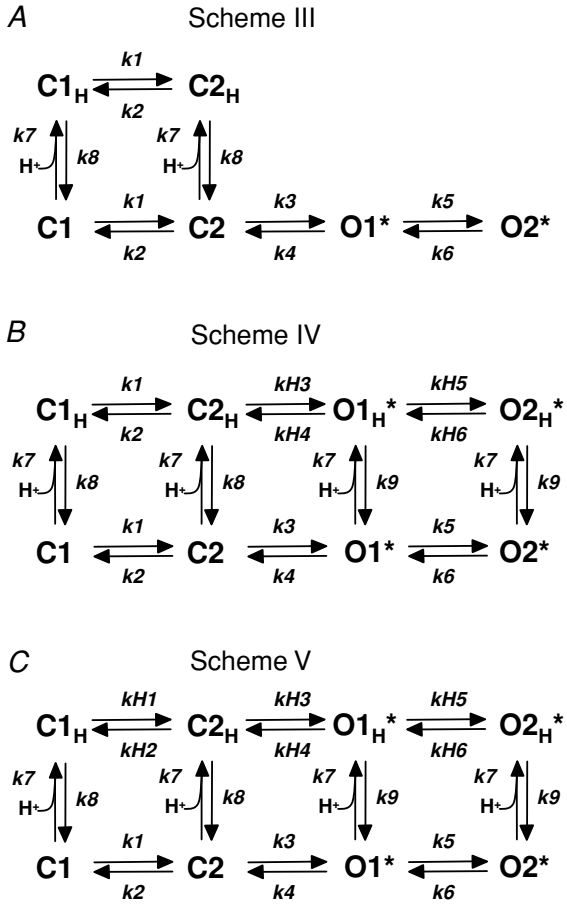


**Figure 8. Conceptual models of $Zn^{2+}$ enhanced proton sensitivity**
*A*, Scheme III is a conceptual model that includes explicit protonation steps from closed states. *B*, Scheme IV is an extension of this model with protonation steps from open and closed states, with pregating rates fixed to be equal for protonated and unprotonated states. *C*, Scheme V is a modification of Scheme IV in which all gating rate constants are allowed to vary independently for protonated and unprotonated closed states. The proton association rate in Scheme V is fixed to that determined from proton concentration jump experiments (Banke *et al.* 2005); all other rates are free parameters in the model. Fitted rate constants are given in Tables 2 and 3.

We first examined conceptual ideas of how $Zn^{2+}$ might influence receptor protonation. We fitted the three models shown in Fig. 8 to our data set from seven patches in which we recorded channels in both control conditions and 300 nM $Zn^{2+}$. This dataset included two patches with no double openings, and which probably contain one active channel. Recordings of channel activity in all patches were segmented into bursts, and the data were pooled and analysed as described in the Methods. Each model was fitted to data in the absence of extracellular $Zn^{2+}$ (i.e. 10 mM tricine) and again in the presence of 300 nM $Zn^{2+}$. We assumed that $Zn^{2+}$ binding had reached equilibrium and was nearly saturating at 300 nM (Low *et al.* 2000). Each model was fitted to single-channel data using the maximum interval likelihood method (MIL, see Methods). All models reproduced our key observations of a change in open probability within a burst and shortening of the mean open time. The mean open time in control conditions was 3.6 ms, and was reduced to 2.1–2.7 ms in 300 nM $Zn^{2+}$ for Schemes III and IV, respectively. Similarly, the open probability within a burst was reduced from 0.60–0.62 in control to 0.29–0.30 in $Zn^{2+}$ for these models. Table 2 summarizes the rate constants derived from the global fits to the data.

Scheme III shows a linear model in which only the closed states can become protonated, with gating rates of the protonated receptor held identical to rates of the unprotonated receptor (Banke *et al.* 2005). All other rates were allowed to vary in the absence and presence of $Zn^{2+}$. The dominant effect of $Zn^{2+}$ on the fitted rate constants in Scheme III was an acceleration of the proton association rate ($k_7$, Table 2); there were more modest changes in channel closing rate ($k_4$), the forward and reverse rate constants for the initial gating step ($k_1$ and $k_2$), and the proton dissociation rate ($k_8$). However, this model is conceptually unsatisfactory because there is no link between the effects of protons and a reduced mean open time, as implied by data in Figs 5 and 6. We subsequently considered providing a direct protonation path from the open state that leads to channel closure, to allow acceleration of channel closure in high proton concentrations through protonation (and closure) of open channels. However, a conceptual disadvantage of

**Table 2. Idealized and segmented current records from the same patches were fitted with the models shown in Fig. 8*A* and *B***

| | Scheme III | | | | Scheme IV | | |
|---|---|---|---|---|---|---|---|
| | Control | 300 nM $Zn^{2+}$ | $Zn^{2+}$/Control | | Control | 300 nM $Zn^{2+}$ | $Zn^{2+}$/Control |
| $k_1$ ($s^{-1}$) | 940 | 2200 | 2.34 | $k_1$ ($s^{-1}$) | 630 | 560 | 0.89 |
| $k_2$ ($s^{-1}$) | 2300 | 5900 | 2.57 | $k_2$ ($s^{-1}$) | 1700 | 2400 | 1.41 |
| $k_3$ ($s^{-1}$) | 2900 | 3500 | 1.21 | $k_3$ ($s^{-1}$) | 2800 | 3000 | 1.07 |
| $k_4$ ($s^{-1}$) | 3000 | 5300 | 1.77 | $k_4$ ($s^{-1}$) | 2500 | 2900 | 1.16 |
| $k_5$ ($s^{-1}$) | 6300 | 5800 | 0.92 | $k_5$ ($s^{-1}$) | 6400 | 6300 | 0.98 |
| $k_6$ ($s^{-1}$) | 900 | 820 | 0.91 | $k_6$ ($s^{-1}$) | 1000 | 1100 | 1.10 |
| $k_7$ ($M^{-1}$ $s^{-1}$) | **1.5e+9** | **1.5e+10** | 10 | $k_7$ ($M^{-1}$ $s^{-1}$) | **3.5e+7** | **2.6e+8** | **7.42** |
| $k_8$ ($s^{-1}$) | 180 | 380 | 2.11 | $k_8$ ($s^{-1}$) | 4.1 | 4.6 | 1.12 |
| | | | | $k_9$ ($s^{-1}$) | 29 | 33 | 1.14 |
| | | | | $kH_3$ ($s^{-1}$) | 820 | 980 | 1.20 |
| | | | | $kH_4$ ($s^{-1}$) | 5200 | 6700 | 1.29 |
| | | | | $kH_5$ ($s^{-1}$) | 5700 | 5100 | 0.89 |
| | | | | $kH_6$ ($s^{-1}$) | 890 | 870 | 0.98 |
| logL/event | 5.12 | 5.00 | — | logL/event | 5.14 | 5.02 | — |

Records from all 7 patches were pooled and fitted simultaneously. First, data obtained in the absence of $Zn^{2+}$ (i.e. in the presence of 10 mM tricine) were fitted, and subsequently the same model was fitted to data recorded from the same 7 patches in the presence of 300 nM extracellular $Zn^{2+}$. The proton concentration was 62 nM (pH 7.3). All loops were constrained in all models to obey microscopic reversibility. Rates in bold indicate more than a 3-fold change in the presence of $Zn^{2+}$. Rate constants are given to two significant digits.

**Table 3. Idealized and segmented current records from the same patches were fitted by Scheme V as shown in Fig. 8C**

| | Scheme V | | |
|---|---|---|---|
| | Control | 300 nM $Zn^{2+}$ | $Zn^{2+}$/Control |
| $k_1$ ($s^{-1}$) | 1100 | 900 | 0.82 |
| $k_2$ ($s^{-1}$) | 2700 | 3200 | 1.19 |
| $k_3$ ($s^{-1}$) | 3800 | 4200 | 1.11 |
| $k_4$ ($s^{-1}$) | 1900 | 2600 | 1.37 |
| $k_5$ ($s^{-1}$) | 6300 | 6500 | 1.03 |
| $k_6$ ($s^{-1}$) | 1200 | 1200 | 1.00 |
| $k_7$ ($M^{-1}$ $s^{-1}$) | 1.4e+9 | 1.4e+9 | — |
| $k_8$ ($s^{-1}$) | **47** | **12** | **0.26** |
| $k_9$ ($s^{-1}$) | **630** | **150** | **0.24** |
| $kH_1$ ($s^{-1}$) | 300 | 610 | 2.03 |
| $kH_2$ ($s^{-1}$) | 750 | 2200 | 2.93 |
| $kH_3$ ($s^{-1}$) | 900 | 820 | 0.91 |
| $kH_4$ ($s^{-1}$) | 5800 | 6700 | 1.16 |
| $kH_5$ ($s^{-1}$) | 5500 | 5000 | 0.91 |
| $kH_6$ ($s^{-1}$) | 1100 | 920 | 0.84 |
| log*L*/event | 5.13 | 5.02 | — |

Records from all 7 patches were pooled and fitted simultaneously. The proton concentration was 62 nM (pH 7.3). All loops were constrained to obey microscopic reversibility; proton association rate was fixed to $1.4 \times 10^9$ $M^{-1}$ $s^{-1}$ (Banke *et al.* 2005); all other rate constants were free parameters during fitting. The ratio of rate constants determined in 300 nM $Zn^{2+}$ to those determined for control conditions (10 mM tricine, no added $Zn^{2+}$) is given in the far right column. Rates in bold show more than a 3-fold change in the presence of $Zn^{2+}$. Rate constants are given to two significant digits.

this approach is the representation of two different events (protonation and channel closure) as a single step. Scheme IV circumvents this problem by separating protonation and channel closing steps. To fit this model, we forced proton association rates for closed and open states to be equal, but allowed proton dissociation rates to differ for open and closed states. This allowed variation of closing rates of protonated and unprotonated channels while maintaining microscopic reversibility; all loops were held in thermodynamic balance during fitting. The primary change in fitted rate constants between control conditions (no $Zn^{2+}$) and 300 nM $Zn^{2+}$ is an enhancement of proton sensitivity that is manifested as a $Zn^{2+}$-induced acceleration of the proton association rate ($k_7$, see Table 2). The $Zn^{2+}$-induced decrease in channel open time reflects the accelerated closing rate for protonated receptors (compare $k_4$ to $kH_4$ in Scheme IV, Table 2).

Schemes III and IV reproduced the expected $Zn^{2+}$-induced reduction in open time, reduction in open probability, increase in occupancy of protonated states, and enhancement of proton sensitivity. Schemes III and IV additionally reproduced the open and closed time histograms (not shown). However, neither of these models provided realistic $IC_{50}$ values for proton inhibition in the absence of $Zn^{2+}$. Simulated $IC_{50}$ values (pH 6.4 and 6.6 for Schemes III and IV, respectively) were considerably less than the experimental value of pH $\approx$ 7.0 (Low *et al.* 2000). One possible explanation for this was the lack of constraint on proton binding rates, which were allowed to vary during fitting. We

therefore examined a new model (Scheme V) in which we fixed the proton association rate to a value measured for NR1/NR2B receptors ($1.4 \times 10^9$ M$^{-1}$ s$^{-1}$; Banke *et al.* 2005), and allowed all other rate constants to vary during the fitting (Fig. 8*C*; Table 3). As observed for Schemes I and II, the magnitude of $Zn^{2+}$-induced changes in rate constants were very similar between mean rate constants determined from fits to data from individual patches and rate constants determined from the global fits to the pooled data (Supplemental Table 1). Scheme V provided an excellent fit to the data (Fig. 9*A*–*D*), accurately represented single-channel dwell time distributions, and reproduced the key changes produced by $Zn^{2+}$ on proton sensitivity.

These $Zn^{2+}$-induced changes in fitted rate constants reproduced the key functional features of $Zn^{2+}$ binding to NR2A. As the proton association rate was held constant, the $Zn^{2+}$-induced increase in proton sensitivity was manifested as a slowing of the proton dissociation rate, which led to an increased fraction of protonated receptors. Scheme V reproduced the $Zn^{2+}$-induced changes in open time and open probability within a burst accurately, and predicted the observed changes in mean open time and open probability within a burst in patches at low pH (Fig. 9*A*). The $Zn^{2+}$-induced decrease in open time reflected the faster closing rate of protonated receptors than unprotonated receptors (compare $k_4$ to $kH_4$ in Table 3). The lower open probability of protonated

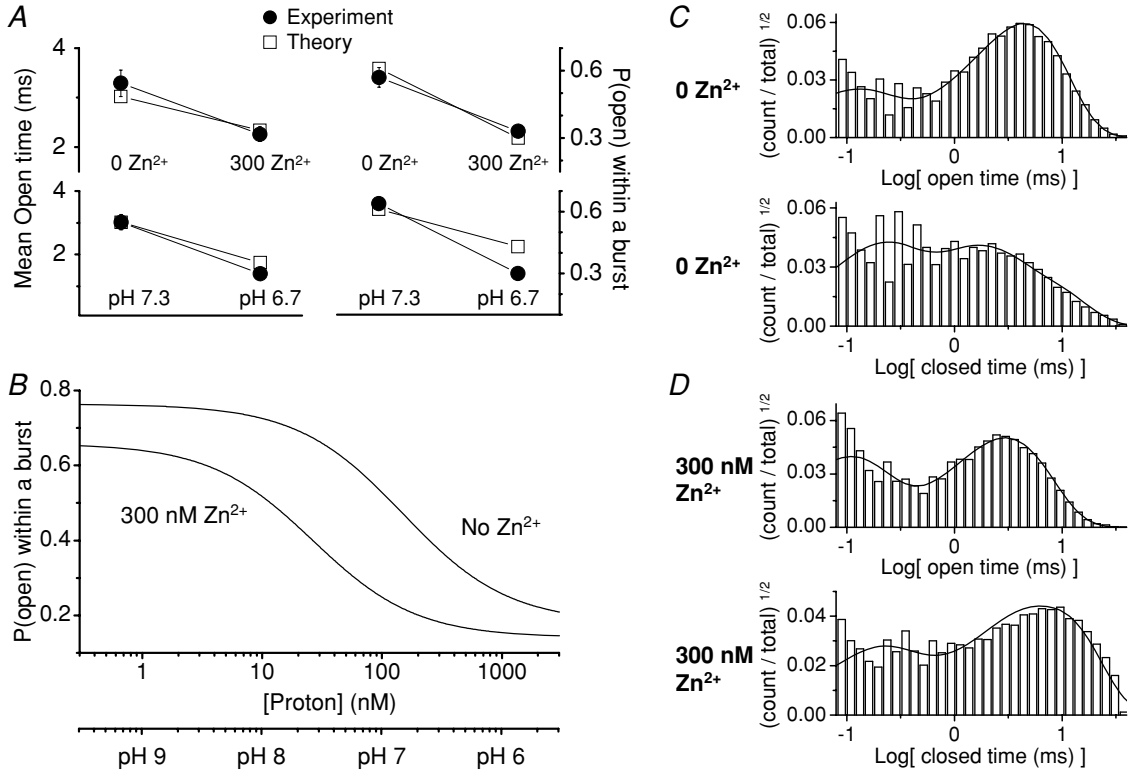


**Figure 9. $Zn^{2+}$ enhancement of proton sensitivity**
*A*, the rate constants determined by fitting Scheme V to single-channel data (Table 3) can reproduce the main features of proton and $Zn^{2+}$ inhibition. The model predictions ('Theory') for mean open time and open probability are plotted compared to the experimental values for each condition. *B*, the model reproduced the effects of $Zn^{2+}$ binding on the proton $IC_{50}$ for the open probability, assessed by fitting the simulated concentration–response data with the equation

$$\text{Open probability} = \text{Maximal open probability}/\left(1 + \left([H^+]/IC_{50}\right)^N\right)$$

where $IC_{50}$ is the concentration that produces a half-maximal response and $N$ is the Hill slope. The fitted proton $IC_{50}$ for this model in the absence of $Zn^{2+}$ was 140 nM (pH 6.9); open probability ranged between 0.19 and 0.76 and the Hill slope was 1.0. The fitted proton $IC_{50}$ for this model in 300 nM $Zn^{2+}$ was 25 nM (pH 7.7); open probability within a burst ranged between 0.14 and 0.66 and the Hill slope was 1.0. *C* and *D*, the fitted rate constants can reproduce the open and closed duration single-channel histograms observed in control conditions (0 $Zn^{2+}$, *C*) and in 300 nM $Zn^{2+}$ (*D*). The superimposed probability density functions are calculated from the global fit of Scheme V across all patches for either the 0 nM $Zn^{2+}$or 300 nM $Zn^{2+}$ data set.

receptors probably involved slower forward rates for gating steps (compare $k_3$ to $kH_3$ in Table 3) in combination with faster channel closing rates. In addition, this model predicted realistic values for the proton sensitivity of the open probability (Fig. 9*B*). Consistent with previously reported effects of $Zn^{2+}$ on proton $IC_{50}$, simulations with fitted rate constants suggest that $Zn^{2+}$ induced a higher apparent affinity for proton inhibition. The predicted proton $IC_{50}$ was 140 nM (pH 6.9) in the absence of $Zn^{2+}$ and 25 nM (pH 7.7) in the presence of 300 nM $Zn^{2+}$. The model predicted that the $K_d$ for proton binding to the closed states is shifted from 35 nM to 10 nM by $Zn^{2+}$; the $K_d$ for proton binding to the open states is shifted from 481 nM to 115 nM by $Zn^{2+}$. The primary shortcoming of this model is the incomplete inhibition predicted by pH (Fig. 9*B*), which is inconsistent with previously reported data (Tang *et al.* 1990; Traynelis & Cull-Candy, 1990; Low *et al.* 2000). This may reflect engagement of other proton-sensitive residues at extremely low pH, or perhaps inaccurate representation of the open probability of protonated receptors due to oversimplification of the gating scheme. One additional caveat with this model is that it does not predict strong correlations between open and shut durations (data not shown), in contrast to observed data. This probably reflects oversimplification of the gating scheme in favour of inclusion of explicit protonation steps.

## Discussion

There are two main findings of this study. First, the inhibition of single-channel currents recorded from recombinant NR1/NR2A NMDA receptors by submicromolar concentrations of extracellular $Zn^{2+}$ and protons appears similar. Second, high affinity $Zn^{2+}$ inhibition of NR2A-containing NMDA receptors is due to a decrease in the mean channel open duration and a decrease in the open probability within a burst of channel activity with no effect on the unitary open channel current amplitude. Kinetic modelling suggests that these effects of $Zn^{2+}$ primarily reflect an enhancement of proton sensitivity. Moreover, the decrease in mean open time may involve an accelerated closing rate for protonated receptors. These findings provide further support for the hypothesis that $Zn^{2+}$ inhibition of NR1/NR2A receptors reflects enhancement of tonic proton inhibition (Choi & Lipton, 1999; Low *et al.* 2000; Zheng *et al.* 2001; Erreger & Traynelis, 2005).

### Mechanism of $Zn^{2+}$-induced inhibition of NR1/NR2A receptors

There are two hypotheses that could account for the similarities in the effects of $Zn^{2+}$ and protons on NR1/NR2A single-channel properties. The first is that $Zn^{2+}$ and protons share a common downstream target, the channel gating machinery, and thus modify each others actions through an allosteric mechanism. The second hypothesis is that $Zn^{2+}$ binding brings about an enhancement in the sensitivity to protons, resulting in an increase in inhibition of $Zn^{2+}$-bound NMDA receptors by physiological concentrations of protons. Multiple lines of evidence in the literature favour the second hypothesis, that zinc binding leads to enhanced sensitivity to protons. First, the presence of 1 $\mu$M zinc shifts the $IC_{50}$ for proton inhibition from pH 7.0 to pH 7.3–7.6 (Choi & Lipton, 1999; Low *et al.* 2000). Second, inhibition by zinc is incomplete even at saturating concentrations and the degree of maximal inhibition is pH dependent, and can be accounted for by a model assuming that $Zn^{2+}$ acts by shifting the $pK_a$ for the proton sensor (Low *et al.* 2000; Zheng *et al.* 2001; Erreger & Traynelis, 2005). Third, the binding of phenolethanolamines to the amino terminal domain of NR2B has been shown to enhance proton sensitivity in much the same way as $Zn^{2+}$ binding to the amino terminal domain of NR2A is hypothesized to enhance proton inhibition (Mott *et al.* 1998; Paoletti *et al.* 2000; Perin-Dureau *et al.* 2002).

Proton sensitivity has previously been studied in detail at the single-channel level for NR1/NR2B receptors and native NMDA receptors. A number of parallels exist between our data and this previous work. For example, we find the models that best describe our data include a protonated arm of the receptor gating scheme (Banke *et al.* 2005). In addition, protons decrease open probability (Traynelis & Cull-Candy, 1991; Banke *et al.* 2005), similar to the effects of $Zn^{2+}$. However, the pH dependence of the mean open channel duration for NR2A-containing receptors differs from NR2B-containing receptors, which show only modest effects of protons on open times (Banke *et al.* 2005). Given the minimal effect of protons on NR1/NR2B open times, previous kinetic modelling did not need to incorporate mechanisms that would accelerate channel closure in low pH solutions to reproduce single-channel data. However, the more prominent effects of protons on open time for NR1/NR2A forced consideration of new potential mechanisms. The addition of protonation paths for open channels seems conceptually reasonable, and suggests that the proton sensor remains accessible and protonatable in open channels for NR1/NR2A. Indeed, the lack of protonation of any states in NR1/NR2B models previously examined might simply reflect a lower proton sensitivity of these states, so low that these steps could be omitted without compromising our ability to describe the data. Thus, we favour a unifying theory between proton sensitivity of NR1/NR2A and NR1/NR2B receptors, with minimal contribution of protonation pathways from open states of NR1/NR2B to inhibition.

Previous studies have shown that alternate RNA splicing of the NR1 subunit can influence both proton and $Zn^{2+}$ inhibition (Traynelis *et al.* 1995, 1998). Inclusion of the highly charged residues encoded by the alternatively splice exon5 reduces the sensitivity to both extracellular $Zn^{2+}$ and protons. We expect the results obtained here to apply to receptors that lack or contain residues encoded by alternative exon5. We predict that although proton binding and unbinding rates will yield lower proton sensitivity in exon5-containing receptors, that saturating concentrations of $Zn^{2+}$ will still enhance the protonation of NR1/NR2A receptors that contain NR1 exon5.

### Comparison to studies of $Zn^{2+}$ inhibition of native NMDA receptors

The functional effects of $Zn^{2+}$ on neuronal NMDA channels of unknown subunit composition have previously been investigated in patches from cultured cortical and hippocampal neurons and at relatively high zinc concentrations ($> 1\,\mu$M) that may induce voltage-dependent channel block in addition to the high affinity voltage-independent inhibition (Christine & Choi, 1990; Legendre & Westbrook, 1990). An additional complication of these early studies is that the high affinity zinc inhibition of NR2A-containing receptors may have been obscured in these experiments by ambient levels of zinc in standard laboratory salt solutions ($\sim$300 nM) (Li *et al.* 1996; Zheng *et al.* 1998) used as controls in the absence of a divalent buffer such as EDTA or tricine. Nonetheless, our results are in part consistent with these studies, which reported that $Zn^{2+}$ causes a decrease in mean channel open time and a decrease in opening frequency.

### Summary

In summary, this study demonstrates that high affinity $Zn^{2+}$ inhibition and proton inhibition of NR1/NR2A NMDA receptors share a common functional signature at the single-channel level. Both protons and extracellular $Zn^{2+}$ decrease the mean channel open duration and the channel open probability without altering the single-channel conductance. In addition, we present strong evidence for a mechanism of $Zn^{2+}$-induced inhibition of NR1/NR2A receptors that involves $Zn^{2+}$ enhancement of tonic proton inhibition.

## References

Ayalon G, Segev E, Elgavish S & Stern-Bach Y (2005). Two regions in the N-terminal domain of ionotropic glutamate receptor 3 form the subunit oligomerization interfaces that control subtype-specific receptor assembly. *J Biol Chem* **280**, 15053–15060.

Ayalon G & Stern-Bach Y (2001). Functional assembly of AMPA and kainate receptors is mediated by several discrete protein–protein interactions. *Neuron* **31**, 103–113.

Banke TG, Dravid SM & Traynelis SF (2005). Protons trap NR1/NR2B NMDA receptors in a nonconducting state. *J Neurosci* **25**, 42–51.

Banke TG & Traynelis SF (2003). Activation of NR1/NR2B NMDA receptors. *Nat Neurosci* **6**, 144–152.

Chen N, Moshaver A & Raymond LA (1997). Differential sensitivity of recombinant N-methyl-D-aspartate receptor subtypes to zinc inhibition. *Mol Pharmacol* **51**, 1015–1023.

Chesler M (2003). Regulation and modulation of pH in the brain. *Physiol Rev* **83**, 1183–1221.

Choi YB & Lipton SA (1999). Identification and mechanism of action of two histidine residues underlying high-affinity $Zn^{2+}$ inhibition of the NMDA receptor. *Neuron* **23**, 171–180.

Christine CW & Choi DW (1990). Effect of zinc on NMDA receptor-mediated channel currents in cortical neurons. *J Neurosci* **10**, 108–116.

Colquhoun D & Hawkes (1995). The principles of the stochastic interpretation of ion-channel mechanisms. In *Single-Channel Recording*, ed. Sakmann B & Neher E. Plenum Press, New York.

Colquhoun D & Sakmann B (1985). Fast events in single-channel currents activated by acetylcholine and its analogues at the frog muscle end-plate. *J Physiol* **369**, 501–557.

Colquhoun D & Sigworth (1995). Fitting and statistical analysis of single-channel records. In *Single-Channel Recording*, ed. Sakmann B & Neher E. Plenum Press, New York.

DeVries SH (2001). Exocytosed protons feedback to suppress the $Ca^{2+}$ current in mammalian cone photoreceptors. *Neuron* **32**, 1107–1117.

Dingledine R, Borges K, Bowie D & Traynelis SF (1999). The glutamate receptor ion channels. *Pharmacol Rev* **51**, 7–61.

Erreger K, Chen PE, Wyllie DJ & Traynelis SF (2004). Glutamate receptor gating. *Crit Rev Neurobiol* **16**, 187–224.

Erreger K, Dravid SM, Banke TG, Wyllie DJ & Traynelis SF (2005*a*). Subunit-specific gating controls rat NR1/NR2A and NR1/NR2B NMDA channel kinetics and synaptic signalling profiles. *J Physiol* **563**, 345–358.

Erreger K, Geballe MT, Dravid SM, Snyder JP, Wyllie DJ & Traynelis SF (2005*b*). Mechanism of partial agonism at NMDA receptors for a conformationally restricted glutamate analog. *J Neurosci* **25**, 7858–7866.

Erreger K & Traynelis SF (2005). Allosteric interaction between zinc and glutamate binding domains on NR2A causes desensitization of NMDA receptors. *J Physiol* **569**, 381–393.

Frederickson CJ, Giblin LJ 3rd, Balaji RV, Masalha R, Zeng Y, Lopez EV, Koh JY, Chorin U, Besser L, Hershfinkel M, Li Y, Thompson RB & Krezel A (2006). Synaptic release of zinc from brain slices: factors governing release, imaging, and accurate calculation of concentration. *J Neurosci Meth* **154**, 19–29.

Gibb AJ & Colquhoun D (1991). Glutamate activation of a single NMDA receptor-channel produces a cluster of channel openings. *Proc Biol Sci* **243**, 39–45.

Gottfried JA & Chesler M (1994). Endogenous $H^+$ modulation of NMDA receptor-mediated EPSCs revealed by carbonic anhydrase inhibition in rat hippocampus. *J Physiol* **478**, 373–378.

Hatton CJ & Paoletti P (2005). Modulation of triheteromeric NMDA receptors by N-terminal domain ligands. *Neuron* **46**, 261–274.

Jackson MB, Wong BS, Morris CE, Lecar H & Christian CN (1983). Successive openings of the same acetylcholine receptor channel are correlated in open time. *Biophys J* **42**, 109–114.

Kay AR (2003). Evidence for chelatable zinc in the extracellular space of the hippocampus, but little evidence for synaptic release of Zn. *J Neurosci* **23**, 6847–6855.

Klein RM & Howe JR (2004). Effects of the lurcher mutation on GluR1 desensitization and activation kinetics. *J Neurosci* **24**, 4941–4951.

Kohda K, Wang Y & Yuzaki M (2000). Mutation of a glutamate receptor motif reveals its role in gating and $\delta 2$ receptor channel properties. *Nat Neurosci* **3**, 315–322.

Legendre P & Westbrook GL (1990). The inhibition of single *N*-methyl-D-aspartate-activated channels by zinc ions on cultured rat neurones. *J Physiol* **429**, 429–449.

Leuschner WD & Hoch W (1999). Subtype-specific assembly of $\alpha$-amino-3-hydroxy-5-methyl-4-isoxazole propionic acid receptor subunits is mediated by their n-terminal domains. *J Biol Chem* **274**, 16907–16916.

Li C, Peoples RW & Weight FF (1996). Proton potentiation of ATP-gated ion channel responses to ATP and $Zn^{2+}$ in rat nodose ganglion neurons. *J Neurophysiol* **76**, 3048–3058.

Low CM, Lyuboslavsky P, French A, Le P, Wyatte K, Thiel WH, Marchan EM, Igarashi K, Kashiwagi K, Gernert K, Williams K, Traynelis SF & Zheng F (2003). Molecular determinants of proton-sensitive N-methyl-D-aspartate receptor gating. *Mol Pharmacol* **63**, 1212–1222.

Low CM, Zheng F, Lyuboslavsky P & Traynelis SF (2000). Molecular determinants of coordinated proton and zinc inhibition of N-methyl-D-aspartate NR1/NR2A receptors. *Proc Natl Acad Sci U S A* **97**, 11062–11067.

Makani S & Chesler M (2007). Endogenous alkaline transients boost postsynaptic NMDA receptor responses in hippocampal CA1 pyramidal neurons. *J Neurosci* **27**, 7438–7446.

Masuko T, Kashiwagi K, Kuno T, Nguyen ND, Pahk AJ, Fukuchi J, Igarashi K & Williams K (1999). A regulatory domain (R1–R2) in the amino terminus of the N-methyl-D-aspartate receptor: effects of spermine, protons, and ifenprodil, and structural similarity to bacterial leucine/isoleucine/valine binding protein. *Mol Pharmacol* **55**, 957–969.

Meddows E, Le Bourdelles B, Grimwood S, Wafford K, Sandhu S, Whiting P & McIlhinney RA (2001). Identification of molecular determinants that are important in the assembly of N-methyl-D-aspartate receptors. *J Biol Chem* **276**, 18795–18803.

Miesenbock G, De Angelis DA & Rothman JE (1998). Visualizing secretion and synaptic transmission with pH-sensitive green fluorescent proteins. *Nature* **394**, 192–195.

Mott DD, Doherty JJ, Zhang S, Washburn MS, Fendley MJ, Lyuboslavsky P, Traynelis SF & Dingledine R (1998). Phenylethanolamines inhibit NMDA receptors by enhancing proton inhibition. *Nat Neurosci* **1**, 659–667.

Naur P, Hansen KB, Kristensen AS, Dravid SM, Pickering DS, Olsen L, Vestergaard B, Egebjerg J, Gajhede M, Traynelis SF & Kastrup JS (2007). Ionotropic glutamate-like receptor $\delta 2$ binds D-serine and glycine. *Proc Natl Acad Sci U S A* **104**, 14116–14121.

Paoletti P, Ascher P & Neyton J (1997). High-affinity zinc inhibition of NMDA NR1-NR2A receptors. *J Neurosci* **17**, 5711–5725.

Paoletti P, Perin-Dureau F, Fayyazuddin A, Le Goff A, Callebaut I & Neyton J (2000). Molecular organization of a zinc binding n-terminal modulatory domain in a NMDA receptor subunit. *Neuron* **28**, 911–925.

Perin-Dureau F, Rachline J, Neyton J & Paoletti P (2002). Mapping the binding site of the neuroprotectant ifenprodil on NMDA receptors. *J Neurosci* **22**, 5955–5965.

Popescu G & Auerbach A (2003). Modal gating of NMDA receptors and the shape of their synaptic response. *Nat Neurosci* **6**, 476–483.

Popescu G, Robert A, Howe JR & Auerbach A (2004). Reaction mechanism determines NMDA receptor response to repetitive stimulation. *Nature* **430**, 790–793.

Qin F (2004). Restoration of single-channel currents using the segmental k-means method based on hidden Markov modeling. *Biophys J* **86**, 1488–1501.

Qin F, Auerbach A & Sachs F (1996). Estimating single-channel kinetic parameters from idealized patch-clamp data containing missed events. *Biophys J* **70**, 264–280.

Salazar G, Craige B, Love R, Kalman D & Faundez V (2005). Vglut1 and ZnT3 co-targeting mechanisms regulate vesicular zinc stores in PC12 cells. *J Cell Sci* **118**, 1911–1921.

Schorge S, Elenes S & Colquhoun D (2005). Maximum likelihood fitting of single channel NMDA activity with a mechanism composed of independent dimers of subunits. *J Physiol* **569**, 395–418.

Smart TG, Hosie AM & Miller PS (2004). $Zn^{2+}$ ions: modulators of excitatory and inhibitory synaptic activity. *Neuroscientist* **10**, 432–442.

Tang CM, Dichter M & Morad M (1990). Modulation of the N-methyl-D-aspartate channel by extracellular $H^+$. *Proc Natl Acad Sci U S A* **87**, 6445–6449.

Taverna F, Xiong ZG, Brandes L, Roder JC, Salter MW & MacDonald JF (2000). The Lurcher mutation of an $\alpha$-amino-3-hydroxy-5-methyl-4-isoxazolepropionic acid receptor subunit enhances potency of glutamate and converts an antagonist to an agonist. *J Biol Chem* **275**, 8475–8479.

Tombaugh GC & Sapolsky RM (1993). Evolving concepts about the role of acidosis in ischemic neuropathology. *J Neurochem* **61**, 793–803.

Traynelis SF, Burgess MF, Zheng F, Lyuboslavsky P & Powers JL (1998). Control of voltage-independent zinc inhibition of NMDA receptors by the NR1 subunit. *J Neurosci* **18**, 6163–6175.

Traynelis SF & Cull-Candy SG (1990). Proton inhibition of N-methyl-D-aspartate receptors in cerebellar neurons. *Nature* **345**, 347–350.

Traynelis SF & Cull-Candy SG (1991). Pharmacological properties and $H^+$ sensitivity of excitatory amino acid receptor channels in rat cerebellar granule neurones. *J Physiol* **433**, 727–763.

Traynelis SF, Hartley M & Heinemann SF (1995). Control of proton sensitivity of the NMDA receptor by RNA splicing and polyamines. *Science* **268**, 873–876.

Ueno S, Tsukamoto M, Hirano T, Kikuchi K, Yamada MK, Nishiyama N, Nagano T, Matsuki N & Ikegaya Y (2002). Mossy fiber $Zn^{2+}$ spillover modulates heterosynaptic N-methyl-D-aspartate receptor activity in hippocampal CA3 circuits. *J Cell Biol* **158**, 215–220.

Vogel MW, Caston J, Yuzaki M & Mariani J (2006). The Lurcher mouse: fresh insights from an old mutant. *Brain Res* **1140**, 4–18.

Williams K (1996). Separating dual effects of zinc at recombinant N-methyl-D-aspartate receptors. *Neurosci Lett* **215**, 9–12.

Wong E, Ng FM, Yu CY, Lim P, Lim LH, Traynelis SF & Low CM (2005). Expression and characterization of soluble amino-terminal domain of NR2B subunit of N-methyl-D-aspartate receptor. *Protein Sci* **14**, 2275–2283.

Wyllie DJ, Johnston AR, Lipscombe D & Chen PE (2006). Single-channel analysis of a point mutation of a conserved serine residue in the S2 ligand-binding domain of the NR2A NMDA receptor subunit. *J Physiol* **574**, 477–489.

Zheng F, Erreger K, Low CM, Banke T, Lee CJ, Conn PJ & Traynelis SF (2001). Allosteric interaction between the amino terminal domain and the ligand binding domain of NR2A. *Nat Neurosci* **4**, 894–901.

Zheng F, Gingrich MB, Traynelis SF & Conn PJ (1998). Tyrosine kinase potentiates NMDA receptor currents by reducing tonic zinc inhibition. *Nat Neurosci* **1**, 185–191.

Zhou Y & Auerbach A (2005). Gating reaction mechanisms for NMDA receptor channels. *J Neurosci* **25**, 7914–7923.

## Acknowledgements

We thank Dr David Wyllie for critical comments on the manuscript. This work was supported by a Howard Hughes Predoctoral Fellowship (K.E.), the NIH (NINDS NS36654, S.F.T.), NARSAD (S.F.T.), and the Michael J. Fox Foundation (S.F.T.).

## Author's present address

K. Erreger: Vanderbilt University Department of Molecular Physiology & Biophysics, 7124 MRBIII, 465 21st Ave S., Nashville, TN 37232, USA.

## Supplemental material

Online supplemental material for this paper can be accessed at:
http://jp.physoc.org/cgi/content/full/jphysiol.2007.143941/DC1
and
http://www.blackwell-synergy.com/doi/suppl/10.1113/jphysiol.2007.143941